Spatial resolution limits for synchrotron-based spectromicroscopy in the mid- and near-infrared

Erika Levenson,[a] Philippe Lerch[b] and Michael C. Martin[a]*

[a]Advanced Light Source Division, Lawrence Berkeley National Laboratory, 1 Cyclotron Road, Berkeley, CA 94720, USA, and [b]Swiss Light Source, Paul Scherrer Institut, 5232 Villigen, Switzerland. E-mail: mcmartin@lbl.gov

Spatial resolution tests were performed on beamline 1.4.4 at the Advanced Light Source in Berkeley, CA, USA, a third-generation synchrotron light source. This beamline couples the high-brightness synchrotron source to a Thermo-Electron Continuμm XL infrared microscope. Two types of resolution tests were performed in both the mid-IR and near-IR. The results are compared with a diffraction-limited spot size theory. At shorter near-IR wavelengths the experimental results begin to deviate from diffraction-limited so a combined diffraction-limit and electron-beam-source-size model is employed. This description shows how the physical electron beam size of the synchrotron source begins to dominate the focused spot size at higher energies. The transition from diffraction-limited to electron-beam-size-limited performance is a function of storage-ring parameters and the optical demagnification within the beamline and microscope optics. The discussion includes how different facilities, beamlines and microscopes will affect the achievable spatial resolution. As synchrotron light sources and other next-generation accelerators such as energy-recovery LINACs and free-electron lasers achieve smaller beam emittances, beta-functions and/or energy spreads, diffraction-limited performance can continue to higher-energy beams, perhaps ultimately into the extreme ultraviolet.

Keywords: infrared; resolution; microscopy; Fourier transform infrared; spectromicroscopy; imaging; diffraction; emittance; microspectroscopy; beamline.

1. Introduction

Synchrotron infrared beamlines provide diffraction-limited spatial resolution for spectromicroscopy with high signal-to-noise ratio (Reffner et al., 1995; Carr et al., 1995; Carr, 2001; Martin & McKinney, 1998, 2001). The synchrotron has 100–1000 times higher brightness than a conventional thermal globar source (Reffner et al., 1995; Carr et al., 1995; Martin & McKinney, 2001; Holman et al., 2003; Dumas & Tobin, 2003; Holman & Martin, 2006), enabling a wide variety of new science at small spatial scales (Holman et al., 2000, 2003; Raab & Martin, 2001; Dumas & Tobin, 2003; Miller et al., 2003; Bertrand et al., 2003; Holman & Martin, 2006; Miller & Dumas, 2006; Li et al., 2006; Keller et al., 2006; Veiseh et al., 2007). We have previously verified the diffraction-limited performance through the mid-IR of the IR beamlines at the Advanced Light Source (ALS), in Berkeley (Levenson et al., 2006). However, as the synchrotron emission wavelength becomes shorter and shorter, the physical size of the electron beam will become the dominant factor for the photon source size.

The source size of a synchrotron light beam can be approximated well by adding in quadrature the effects of diffraction, the electron beam size and the projected size of the emitting region (Hirschmugl, 1994; Reffner et al., 1995; Carr et al., 1995; Carr, 2001). This source is then imaged to a focused spot on a sample via beamline optics that have an overall demagnification factor, m. In practice, we have found that after all the beamline collection, collimation and refocusing optics, the effects of diffraction and electron beam size dominate over the projected size of the emitting region, so for this analysis we neglect the latter. The spot size can therefore be written as

$$m\left[(d_R\lambda)^2 + \sigma_t^2\right]^{1/2}, \qquad (1)$$

where d_R is a diffraction limit factor (depends on which resolution model is chosen, as described later), λ is the wavelength of light, and σ_t is the transverse synchrotron electron beam size. As both the electron and photon beams are usually measured and approximated as Gaussian in profile, one must use consistent Gaussian line-width definitions (such

as σ or full width at half-maximum, FWHM) in applying (1). In a synchrotron, the transverse electron beam size is given by

$$\sigma_{t} = \left[\beta_{t}\varepsilon_{t} + \eta_{t}^{2}(\sigma_{E}/E)^{2}\right]^{1/2}, \quad (2)$$

where β_{t} is the beta-function, ε_{t} is the emittance, η_{t} is the dispersion (all transverse to the direction of the electron beam, t can be x or y), and σ_{E}/E is the energy spread (Kim, 1989). These parameters are specific to each storage ring, its operating conditions, and the specific location within the magnetic lattice that the light is being emitted from. These parameters and thus the electron beam sizes in the x and y directions for any specific synchrotron beamline are well known for normal storage-ring operations and typically can be found in the machine data sections of individual light source web sites.

2. Experiment

We performed lateral resolution testing experiments as a function of wavelength in the mid- and near-IR at ALS beamline 1.4.4. A Thermo-Electron Continuμm XL microscope is installed on this beamline along with a Thermo-Electron Nexus 870 FTIR bench which has been modified with an offset laser scanner (similar to the newer Nexus 8700 model). The light from the synchrotron is collected from the 1.4 port using 10 mrad vertical × 40 mrad horizontal collection optics. The front-end optics refocus with a 1:1 image at a diamond window which lets the light beam exit the ultra-high vacuum. A pair of cylindrical mirrors are used to collimate the x and y directions of this source before steering the light into the emission port of the FTIR bench. The light is modulated and then passed through the IR microscope and is focused onto the sample using all reflective 15× or 32× Cassegrain objectives with numerical apertures (NA) of 0.58 and 0.65, respectively. The results presented here were obtained using the 32× objective; however, very similar results were also obtained using the 15× objective. The sample stage is a Prior Scientific H101 stage which is computer controlled with step sizes as small as 0.1 μm. All measurements were carried out in reflection mode without any apertures in the light path, and the results presented here detail the y-direction cross sections of the focused spot.[1]

[1] We chose the y direction because the x direction does not fill the full NA of the objective in the reflection mode in this microscope. This (and possibly other beamline optical effects) causes the y direction to have an experimentally measured better focus than the x direction, so the y direction should be closer to diffraction-limited with the NA stated for the objective.
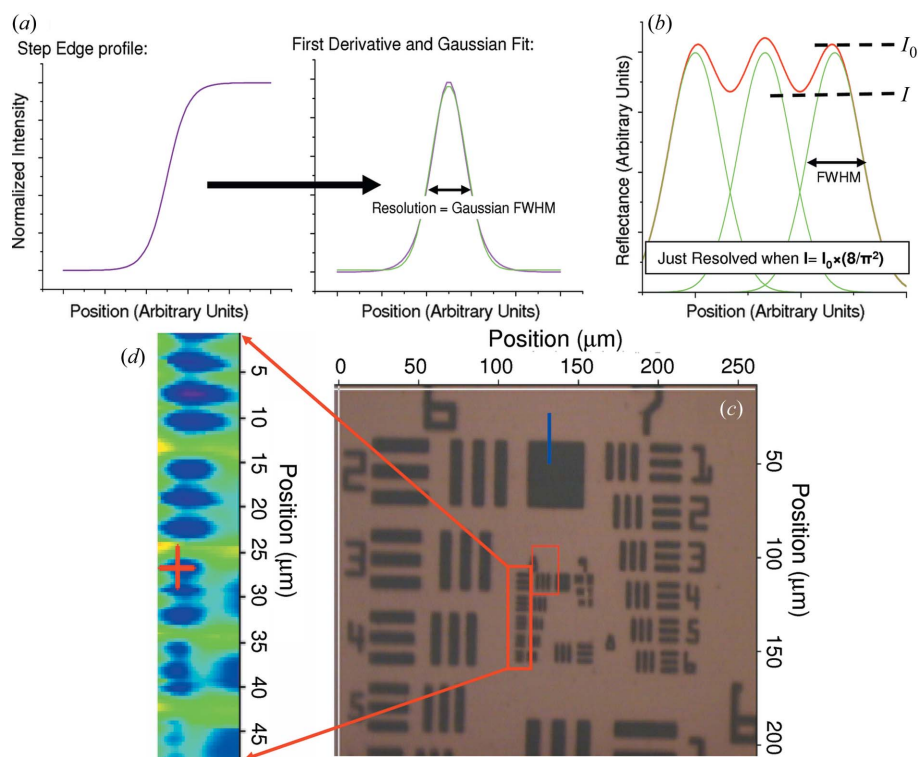

Figure 1
Resolution test definitions. (a) The step-edge resolution test fits a Gaussian function to the first derivative of the measured profile. Resolution is given by the FWHM of the Gaussian. (b) The imaging resolution test uses Rayleigh's criterion to determine whether the peaks are resolved. (c) A micrograph of the USAF 1951 3-Bar Resolving Test Chart. The blue line indicates where the line scan was performed over the edge of the larger square for the step-edge tests. The red box shows group 8 of the test chart where an imaging test example shown in (d) was obtained.

We previously published mid-IR resolution test results showing the resolution is indeed diffraction-limited (Levenson et al., 2006), so for this study we concentrate on the near-IR. An MCT-A* detector was used for wavenumbers ranging from 2000 cm^{-1} to 7000 cm^{-1}. The MCT-A* was swapped with the InGaAs detector to study wavenumbers from 5000 cm^{-1} to 11000 cm^{-1}. A CaF$_2$ beam-splitter was used to cover this entire range.

Spatial resolution tests were performed using a high-resolution USAF 1951 3-Bar Resolving Test Chart (MIL-STD-150A, §5.1.1.7; also see http://www.efg2.com/Lab/Image Processing/TestTargets/) from Applied Image Inc. (Rochester, NY, USA). The USAF resolution test sample has a chrome metal coating on a glass substrate with the resolution test structures patterned in a negative image up to a frequency of 512 cycles mm^{-1} (smallest is group 9, element 3).

Two types of resolution tests were performed. The first is a step-edge (or knife-edge) test. The test is performed stepping the sample from a position where the IR beam is focused on the reflective metal coating to where the beam is focused on the absorbing glass pattern (see Fig. 1c). A spectrum is acquired at each point and a profile of the reflectivity as a function of position and wavelength is obtained. The first derivative of the profile is calculated and fit to a Gaussian function. The FWHM of the Gaussian fit determines the resolution as demonstrated in Fig. 1(a) (Russ, 2002).

The second type of resolution test, whose definition is shown graphically in Fig. 1(b), is an imaging resolution test carried out by scanning across three bars of the same width and distance apart. Once a reflectance profile is obtained *via* a line map across a set of three bars, Rayleigh's criterion (Rayleigh, 1879; Hecht, 1998; Born & Wolf, 1999) is used to determine whether the bars are resolved or not. As shown in Fig. 1(b), Rayleigh's criterion states that if the minimum intensity between two peaks (I) is less than $8/\pi^2$ of the intensity of the peaks (I_0), then the bars are resolved.

These two definitions are well known from the literature; however, it is important to note that they yield different numerical results since they are based on different definitions. The Rayleigh imaging criterion will give a higher resolution than the FWHM step-edge analysis by a factor of 1/2 (half maximum) to $8/\pi^2$, which is 0.617.

Analyses were completed for wavelengths from 1.11 μm to 6.5 μm for the imaging resolution tests and between 0.91 μm and 5 μm for the step-edge resolution tests.

3. Step-edge resolution test results

The MCT-A* detector was used for wavelengths from 1.43 to 5 μm and the InGaAs detector and the CaF$_2$ beam-splitter were used for wavelengths from 0.91 to 2 μm. The step-edge tests were performed using the 32× objective. Example measured profiles for each analyzed wavelength are shown in the inset of Fig. 2. The derivative of each line profile was fit to a Gaussian, and Fig. 2 plots FWHM resolution *versus* wave-
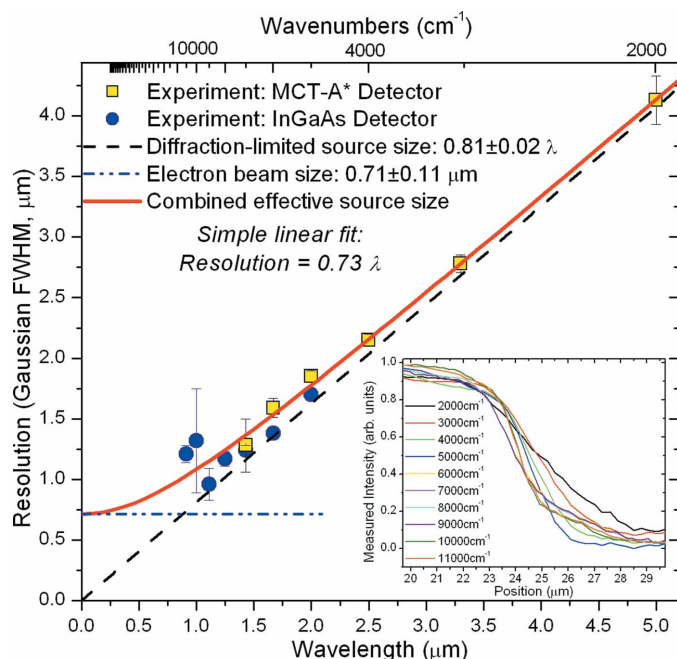

Figure 2
Step-edge resolution test results as a function of wavelength. The FWHM resolution was measured using two detectors to cover the mid- and near-IR spectral ranges. A fit of the data to the effective source size discussed in the text is shown in red, with the two components of the fit, diffraction and electron beam source size, shown with dashed lines. Inset: example raw data of step-edge profiles.

length for both detectors. A simple linear fit to the data is reasonable and yields a resolution for the synchrotron source of $(0.73 \pm 0.04)\lambda$.

This, however, does not follow the theoretical diffraction limit as the intercept of this linear fit does not pass through the origin; therefore it underestimates the slope of the real data, plus the fit becomes worse at shorter wavelengths. An improved and more physically meaningful fit is obtained by using equation (1), which includes the effects of diffraction and the physical size of the electron beam. In this case the best fit results in the diffraction portion of the data given by $(0.81 \pm 0.02)\lambda$, with a demagnified electron beam size of 0.71 ± 0.11 μm. Demagnification shall be discussed further in the paper.

4. Imaging resolution test results

Imaging tests were performed with the synchrotron source with both objectives. Analyses based on Rayleigh's criterion were completed at wavelengths between 6.5 and 1.11 μm. The lower panels in Fig. 3 show Gaussian fits to the profiles of the smallest bars for 7000 cm^{-1} ($\lambda = 1.43$ μm) and 9000 cm^{-1} ($\lambda = 1.11$ μm). Only the 9000 cm^{-1} profile meets Rayleigh's criterion of being resolved. The measured resolutions of all wavelengths analyzed are presented in Fig. 3. A simple linear fit to the data yields a resolution of $(0.45 \pm 0.02)\lambda$.

Again, however, this simple linear fit does not adequately follow the data points particularly at shorter wavelengths, nor does it intercept the origin. The experimental imaging data show more clearly the deviation from a simple diffraction-limited spot size at short wavelengths. An improved fit is found using equation (1) with the diffraction portion of the data given by $(0.47 \pm 0.01)\lambda$ and a demagnified electron beam size of 0.51 ± 0.06 μm.

5. Analysis

As noted above, the step-edge and imaging tests use different resolution definitions and the results should be different by a factor of 0.617. Indeed, we find that the diffraction portion of the best fits to equation (1) are different by a factor of 0.59 ± 0.03 and the electron beam size portions of the fits are different by a factor of 0.72 ± 0.20. Both differences match the ideal difference factor of 0.617 within the error bars and so we conclude that the two resolution tests give consistent results.

The electron beam source size for the 1.4 (22.6°) bending magnet port at the ALS is $\sigma_x = 65$ μm and $\sigma_y = 52$ μm (see ALS Storage Ring Parameters, http://www.als.lbl.gov/als/techspecs/srparameters.html). These are 1σ values, and the FWHM beam size is 2.35 times larger (Russ, 1986). Thus, the electron beam size is 153 μm in the horizontal and 122 μm in the vertical dimension.

The demagnification factor m for the 1.4 beamline is given by the ratio of the focal distance of the collimating mirror to the focal distance of the microscope objective focusing the light onto the sample. We use a 300 mm-radius (150 mm focal distance) cylindrical mirror to collimate the 40 mrad hori-
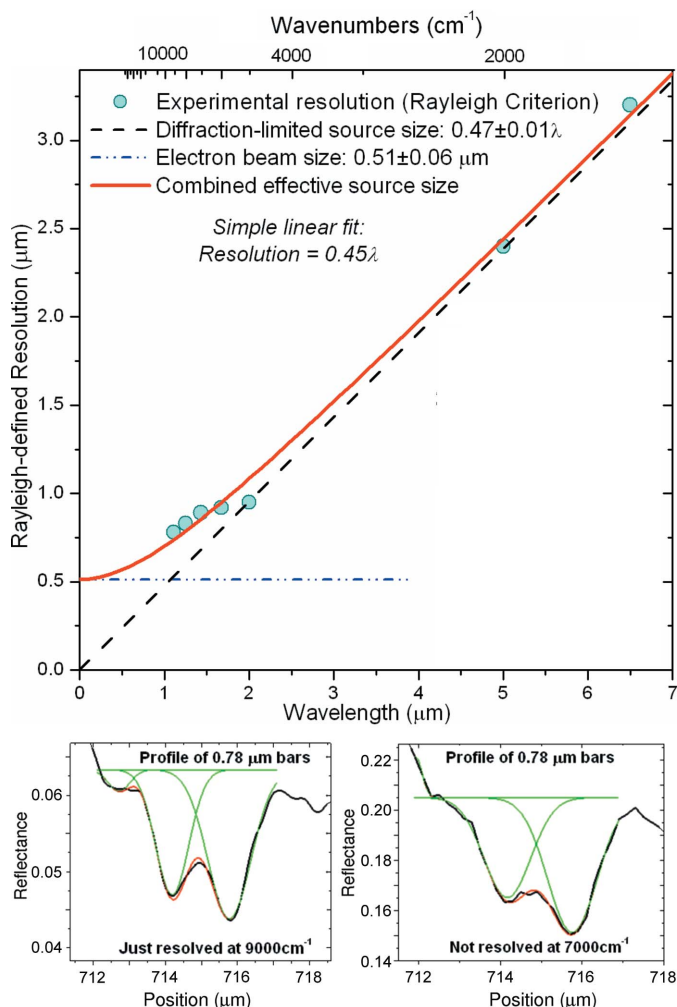
Figure 3
Imaging resolution test results as a function of wavelength. A fit of the data to the effective source size discussed in the text is shown in red, with the two components of the fit, diffraction and electron beam source size, shown with dashed lines. The lower figures show example profiles of the smallest bars at wavelengths of 1.11 µm (just resolved) and 1.43 µm (not resolved) and the corresponding Gaussian fits.

zontal to a 6 mm beam size. In the vertical, we collimate the 10 mrad beam with a 1200 mm-radius (600 mm focal distance) cylinder to again achieve a 6 mm beam size. This 6 mm × 6 mm beam is modulated by the FTIR interferometer, and passes through the infrared microscope to the Cassegrain objective which focuses the light onto the sample. The Cassegrain expands the beam with the secondary mirror, followed by focusing with the larger primary mirror. For simplicity, instead of following the complexities of the Cassegrain, we can mentally substitute the Cassegrain for a simple thin lens, whose focal length is the distance it takes to focus a 6 mm beam to a point using the correct NA value of the Cassegrain. Thus the effective focal distance to the sample (the distance from the sample at which the input beam is 6 mm in size based on the NA of the objective, which would be the focal length of this substitute thin lens) is 3.5 mm for the $32\times$ and 4 mm for the $15\times$ objective based on their NAs of 0.65 and 0.58, respectively.

The beamline 1.4.4 optics image the vertical synchrotron emission to the y direction on the sample stage, which is the direction in which the spot-size measurements are detailed above. The magnification factor for the $32\times$ objective is therefore $m = 171$, and thus we would predict that the FWHM electron beam size of 122 µm is imaged onto the sample stage to 0.71 µm FWHM. Or, using the Rayleigh criterion, the imaged beam size is 0.44 µm. These values are in good agreement with the experimental data of the demagnified electron beam source size fits of 0.71 ± 0.11 µm and 0.51 ± 0.06 µm for the two resolution definitions, respectively.

The usual Rayleigh criterion definition for diffraction-limited lateral resolution is that two adjacent points are just resolved when the centers of their Airy discs are separated by the central Airy disc radius. For an ideal objective (and identical condenser), this limit is given by $1.22\lambda/2NA$. The imaging definition Rayleigh criterion that we defined in Fig. 1(b), however, is when the central Airy discs of an adjacent point are separated by half of their radius, so here the Rayleigh diffraction-limited resolution is $1.22\lambda/4NA$. For the $32\times$ objective with NA = 0.65, we therefore expect the diffraction-limited performance of this objective to be 0.47λ. This is in excellent agreement with the fit to our measured data of $(0.47 \pm 0.01)\lambda$.

6. Resolution performance of different synchrotron beamlines

The achievable transverse resolution of a given synchrotron beamline is a combination of the beamline optics (demagnification factor) and the electron beam source size which is dependent on the specific machine and photon port parameters. The demagnification factor achievable depends not only on the front-end collection optics but also on the final focusing objective in the IR microscope. The Thermo-Electron $15\times$ and $32\times$ objectives have relatively large NAs, whereas the Bruker Optics $15\times$ and $36\times$ objectives have longer working distances but smaller NAs of 0.4 and 0.5, respectively. The effective focal lengths for a 6 mm input beam for these two objectives will be 6.9 mm and 5.2 mm, respectively, which will yield smaller magnification factors for the same front-end optics, and therefore the electron-beam source demagnified on the sample stage using these objectives will be factors of 2 and 1.5 larger. This means that the effects of the electron beam source size will start at longer wavelengths and will limit the ultimate lateral spatial resolution achievable. If we were to use the Bruker $15\times$ objective (NA = 0.4) on the ALS IR beamline with all other optics being the same, we should obtain a spot size given by 0.76λ for the diffraction limit, and a 0.88 µm imaged electron beam size. Other Cassegrain objectives are available from, for example, Ealing Catalog Inc. (Rocklin, CA, USA) with higher and lower magnifications ($15\times$ up to $74\times$) and NAs (0.28 up to 0.65, respectively). Examples of the predicted resolution as a function of wavelength using different NA objectives are plotted in Fig. 4. The choice of objective for a given beamline and/or experiment will there-
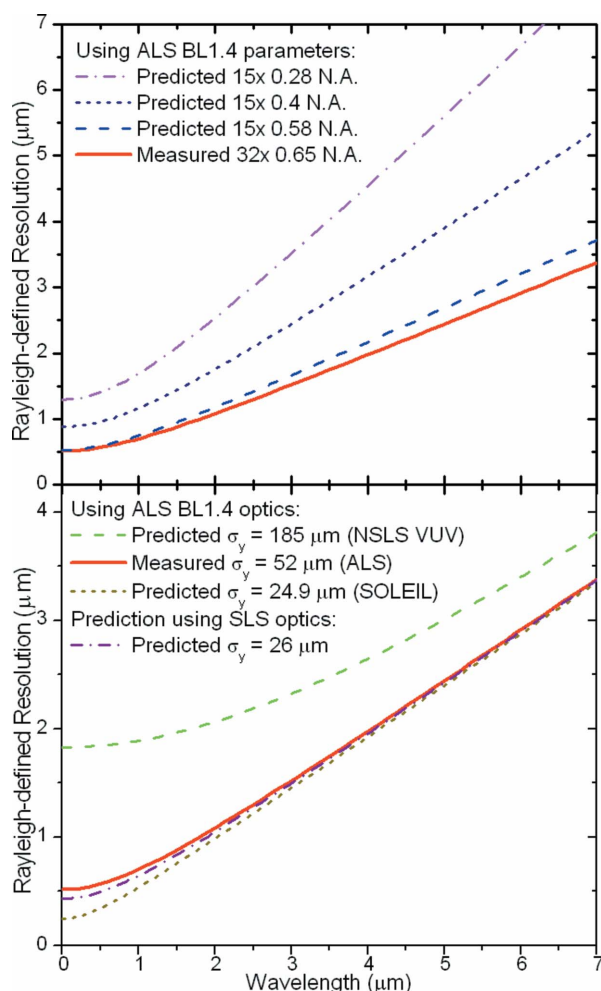
Figure 4
Upper panel: the predicted change in the resolution when using lower numerical aperture objectives. Lower panel: the predicted change in the resolution owing to the different electron beam source sizes at different synchrotron light sources.

fore be a trade-off between higher spatial resolution and greater working distance.

The vertical electron beam source size at the ALS beamline 1.4 port is $\sigma_y = 52\,\mu m$. If this beamline was placed on the smallest source size port at the ALS (x.2 or x.3 ports), the vertical electron beam size is only $\sigma_y = 15\,\mu m$, or a factor of 3.5 smaller. This would have minimal effect on the resolution in most of the mid-IR, but the diffraction-limited performance would extend into the near-IR and a significant improvement in resolution could be achieved for wavelengths shorter than about 2 μm. If the same beamline was built at the NSLS VUV ring (a second-generation synchrotron which has similar IR microscopy beamlines with similar IR microscopes), the bending-magnet vertical electron beam source size is $\sigma_y = 185\,\mu m$ (see *VUV Storage Ring Parameters*, http://www. nsls.bnl.gov/facility/accelerator/vuv/vuv_parameters.pdf), or about 3.5 times larger than the ALS 1.4 port. In this case the electron beam source size will play a more dominant role in the total effective resolution, yielding about 0.5 μm larger spot size (a 25% increase) at $\lambda = 5\,\mu m$ (2000 cm^{-1}), extending to

1 μm larger spot size (double) at $\lambda = 2\,\mu m$ (5000 cm^{-1}) compared with ALS beamline 1.4. An IR microscopy beamline is being built at the new SOLEIL synchrotron (France) which will use the same Continuμm microscope. The planned source size for the port to be used for IR at SOLEIL is $\sigma_y = 24.9\,\mu m$ (see *SOLEIL Parameters at the Source Points*, http://www.synchrotron-soleil.fr/portal/page/portal/Source Accelerateur/ParametresPointsSources), so, assuming similar magnification optics to the ALS, the diffraction-limited performance will continue to wavelengths shorter than 1 μm (10000 cm^{-1}). Fig. 4 presents these comparisons graphically.

The source size at the IR port currently being commissioned at the Swiss Light Source (SLS) storage ring is expected to be $\sigma_x = 52\,\mu m$ and $\sigma_y = 26\,\mu m$. Radiation is transported with one-to-one optics through a diamond, Si or BaF_2 window into a mirror box which collimates the beam and steers it to the beam-splitter of a FTIR spectrometer. The magnification factor m at the SLS IR beamline is 86 (with a 0.58 NA objective) and 82 (with a 0.61 NA objective). This means that the $\sigma_y = 26\,\mu m$ vertical electron beam size will be imaged to the sample with a FWHM of 0.7 μm, or 0.43 μm using the Rayleigh definition. These values are very close to those measured at the ALS, so we would predict very similar resolution capabilities assuming the use of a similar microscope objective (shown in Fig. 4).

The natural vertical angle of the emitted photon beam is a function of wavelength and will decrease as the wavelength becomes shorter. This will become smaller than the collected angle of a given beamline and therefore care must be taken to correctly calculate the demagnification factor m as the photon energy goes beyond the infrared regime. The under-development NSLS-II storage ring is planned to perform at close to the theoretical minimum emittance (Kim, 1989; see also *Summary of NSLS-II Source Properties*, http://www.bnl.gov/nsls2/project/source_properties.asp) possible for a storage ring. The source size in the bending-magnet ports will be $\sigma_x = 44.2\,\mu m$ and $\sigma_y = 15.7\,\mu m$. This is almost a factor of two smaller vertical beam size than SOLEIL, and so it should be possible to extend the diffraction-limited performance to approximately $\lambda = 400\,nm$ in the visible. Different focusing optics could extend this range even further towards the VUV.

7. Conclusions

We have presented careful measurements of the lateral spatial resolution at ALS beamline 1.4.4 and have found that they agree very well with the theoretical resolution given by the optical magnification and electron beam source size. A functional form of the beam size is used to fit the measured data, and is then used to show how the resolution performance will scale as a function of selected optics (numerical aperture of the microscope objective) and as a function of electron beam size for different example synchrotrons. Beamline designers can use these results to help balance throughput, spatial resolution and working distance requirements of their user programs. As accelerator beam sizes become smaller in

newer machines, the diffraction-limited performance can be extended to frequencies above the IR.

References

Bertrand, L., Doucet, J., Dumas, P., Simionovici, A., Tsoucaris, G. & Walter, P. (2003). *J. Synchrotron Rad.* **10**, 387–392.

Born, M. & Wolf, E. (1999). *Principles of Optics*, p. 371. Cambridge University Press.

Carr, G. L. (2001). *Rev. Sci. Instrum.* **72**, 1613.

Carr, G. L., Reffner, J. A. & Williams, G. P. (1995). *Rev. Sci. Instrum.* **66**, 1490.

Dumas, P. & Tobin, M. J. (2003). *Spectrosc. Eur.* **15**, 17–23.

Hecht, E. (1998). *Optics*, p. 416. New York: Addison Wesley Longman.

Hirschmugl, C. J. (1994). PhD thesis, Yale University, USA.

Holman, H.-Y. N. & Martin, M. C. (2006). *Adv. Agron.* **90**, 79–127.

Holman, H.-Y. N., Martin, M. C., Blakely, E. A., Bjornstad, K. & McKinney, W. R. (2000). *Biopolym. Biospectrosc.* **57**, 329–335.

Holman, H.-Y. N., Martin, M. C. & McKinney, W. R. (2003). *Spectroscopy*, **17**, 139–159.

Keller, L. P. *et al.* (2006). *Science*, **314**, 1728–1731.

Kim, K.-J. (1989). *AIP Conf. Proc.* **184**, 565.

Levenson, E., Lerch, P. & Martin, M. C. (2006). *Infrared Phys. Technol.* **49**, 45–52.

Li, Z. Q., Wang, G. M., Sai, N., Moses, D., Martin, M. C., Di Ventra, M., Heeger, A. J. & Basov, D. N. (2006). *Nano Lett.* **6**, 224–228.

Martin, M. C. & McKinney, W. R. (1998). *Proc. Mater. Res. Soc.* **524**, 11.

Martin, M. C. & McKinney, W. R. (2001). *Ferroelectrics*, **249**, 1–10.

Miller, L. M. & Dumas, P. (2006). *Biochim. Biophys. Acta*, **1758**, 846–857.

Miller, L. M., Smith, G. D. & Carr, G. L. (2003). *J. Biol. Phys.* **29**, 219–230.

Raab, T. K. & Martin, M. C. (2001). *Planta*, **213**, 881–887.

Rayleigh, Lord (1879). *Philos. Mag.* **8**, 261–274.

Reffner, J. A., Martoglio, P. A. & Williams, G. P. (1995). *Rev. Sci. Instrum.* **66**, 1298.

Russ, J. C. (1986). *Practical Stereology*, p. 9. New York: Plenum.

Russ, J. C. (2002). *The Image Processing Handbook*, p. 320. Boca Raton: CRC Press.

Veiseh, M., Veiseh, O., Martin, M. C., Bertozzi, C. & Zhang, M. (2007). *Biosens. Bioelectron.* **23**, 253–260.